



Received: 30 November 2013 – Accepted: 3 December 2013 – Published: 13 December 2013

Correspondence to: A. Levermann (anders.levermann@pik-potsdam.de)

Published by Copernicus Publications on behalf of the European Geosciences Union.

**ESDD**

4, 1117–1168, 2013

---

**Antarctic  
ice-discharge from  
SeaRISE  
response-functions**

A. Levermann et al.

---

Title Page

Abstract

Introduction

Conclusions

References

Tables

Figures



Back

Close

Full Screen / Esc

Printer-friendly Version

Interactive Discussion



## Abstract

The largest uncertainty in projections of future sea-level change results from the potentially changing dynamical ice discharge from Antarctica. Basal ice-shelf melting induced by a warming ocean has been identified as a major cause for additional ice flow across the grounding line. Here we derive dynamic ice-sheet response functions for basal ice-shelf melting for four different Antarctic drainage regions using experiments from the Sea-level Response to Ice Sheet Evolution (SeaRISE) intercomparison project with five different Antarctic ice-sheet models. Under the assumptions of linear-response theory we project future ice-discharge for each model, each region and each of the four Representative Concentration Pathways (RCP) using oceanic temperatures from 19 comprehensive climate models of the Coupled Model Intercomparison Project, CMIP-5, and two ocean models from the EU-project Ice2Sea. The uncertainty in the climatic forcing, the oceanic response and the ice-model response is combined into an uncertainty range of future Antarctic ice-discharge induced from basal ice-shelf melt. The uncertainty range we derived for the Antarctic contribution to global sea-level rise from 1992 to 2011 is in full agreement with the observed contribution for this period if we use the three ice-sheet models with an explicit representation of ice-shelf dynamics and account for the time delayed warming of the oceanic subsurface compared with the surface air temperature. The median of the additional ice-loss for the 21st century (Table 6) is 0.07 m (66 %-range: 0.02–0.14 m; 90 %-range: 0.0–0.23 m) of global sea-level equivalent for the low-emission RCP-2.6 scenario and 0.09 m (66 %-range: 0.04–0.21 m; 90 %-range: 0.01–0.37 m) for the strongest RCP-8.5 if models with explicit ice-shelf representation are applied. These results were obtained using a time delay between the surface warming signal and the subsurface oceanic warming as observed in the CMIP-5 models. Without this time delay the values increase to 0.09 m (66 %-range: 0.04–0.17 m; 90 %-range: 0.02–0.25 m) for RCP-2.6 and 0.15 m (66 %-range: 0.07–0.28 m; 90 %-range: 0.04–0.43 m) for RCP-8.5. Our results are scenario dependent which is most visible in the upper percentiles of the distribution, i.e. highest

## Antarctic ice-discharge from SeaRISE response-functions

A. Levermann et al.

Title Page

Abstract

Introduction

Conclusions

References

Tables

Figures



Back

Close

Full Screen / Esc

Printer-friendly Version

Interactive Discussion



contributions to sea level rise. All probability distributions, as provided in Fig. 12, are highly skewed towards high values. The applied ice-sheet models are coarse-resolution with limitations in the representation of grounding-line motion. However, we find the main uncertainty to be introduced by the external forcing to the ice-sheets, i.e. the climatic and oceanic uncertainty dominate. The scaling coefficients for the four different drainage basins provide valuable information for further assessments of future Antarctic ice discharge.

## 1 Introduction

The future evolution of global mean and regional sea-level is important for coastal planning and associated adaptation measures. The Fourth Assessment Report (AR4) of the Intergovernmental Panel on Climate Change (IPCC) provided sea-level projections explicitly excluding changes in dynamic ice-discharge, i.e. additional ice flow across the grounding line, from both Greenland and Antarctica (Solomon et al., 2007). These contributions might however be significant for the next century which would influence global mean (Van den Broeke et al., 2011) as well as regional sea level changes (Mitrovica et al., 2009), especially since contribution from the ice sheets are clearly relevant on longer time scales (Levermann et al., 2013). While the part of the ice-sheet directly susceptible to warming ocean waters on Greenland is limited, marine ice sheets in West Antarctica alone have the potential to elevate sea level globally by several meters (Bamber et al., 2009). Previous projections of the Antarctic ice-sheet mass-balance have used fully coupled climate-ice-sheet models (Huybrechts et al., 2011; Vizcaino et al., 2010, e.g.). These simulations include feedbacks between the climate and the ice sheet and thereby provide very valuable information especially on multi-centennial time scale. However, on shorter decadal to centennial time scales the direct climatic forcing is likely to dominate the ice-sheet evolution. For 21st-century projections it is thus appropriate to apply the output of comprehensive climate models as external forcing

### Antarctic ice-discharge from SeaRISE response-functions

A. Levermann et al.

Title Page

Abstract

Introduction

Conclusions

References

Tables

Figures



Back

Close

Full Screen / Esc

Printer-friendly Version

Interactive Discussion



to the ice sheet, neglecting feedbacks while possibly improving on the accuracy of the forcing anomalies. Here we follow this approach.

In order to meet the relatively high standards that are set by climate models for the oceanic thermal expansion and glacier- and ice-cap models which use the full range of state-of-the-art climate projections, it is desirable to use a set of different ice-sheet models to increase the robustness in the projections of Antarctica's future sea-level contribution. While changes in basal lubrications, ice-softening from surface warming and changes in surface elevation through altered precipitation can affect dynamic ice-discharge from Antarctica, changes in basal melt underneath the ice shelves will likely be the dominant driver of changes in dynamic ice loss.

Here we combine the dynamic response of five different Antarctic ice-sheet models to changes in basal ice-shelf melt with the full uncertainty range of future climate change for each of the Representative Concentration Pathways (RCP, Moss et al., 2010; Meinshausen et al., 2011a) using the current simulations from the Coupled Model Intercomparison Projection, CMIP-5 (Taylor et al., 2012). To this end we derive response functions for the five ice-sheet models from a standardized melting experiment (M2) from the Sea-level Response to Ice Sheet Evolution (SeaRISE) inter-comparison project (Bindschadler et al., 2013). This community effort gathers a broad range of structurally different ice-sheet models to perform a climate-forcing sensitivity study for both Antarctica (Nowicki et al., 2013a) and Greenland (Nowicki et al., 2013b). A suite of prescribed numerical experiments on a common set of input data represents different types of climate input, namely enhanced sub-shelf melting, enhanced sliding and surface temperature increase combined with enhanced net accumulation.

The spread in the response of the participating models to these experiments originates from differences in the stress-balance approximations, the treatment of grounding line motion, the implementation of ice-shelf dynamics, the computation of the surface-mass balance, and in the computational demand which sets strong limits on the spin-up procedure. Our approach allows to identify the sensitivity of the response of coarse-resolution ice-sheet models to changes in different types of climate-related

**Antarctic  
ice-discharge from  
SeaRISE  
response-functions**

A. Levermann et al.

Title Page

Abstract

Introduction

Conclusions

References

Tables

Figures



Back

Close

Full Screen / Esc

Printer-friendly Version

Interactive Discussion



boundary conditions. An interpolation analysis of the results is performed in (Bind-  
schadler et al., 2013) in order to provide a best-guess estimate of the future sea-level  
contribution from the ice sheets. The framework of linear response theory has been  
used before, for example to generalize climatic response to greenhouse gas emissions  
(Good et al., 2011).

## 2 Brief description of the ice-sheet and ocean models

All ice-sheet models are described in detail by Bind-  
schadler et al. (2013) (Table 2). Here we provide a brief summary referring to relevant publications from which more  
detailed descriptions can be obtained. All model's applied are continental ice-sheet  
models and coarse in resolution. As a consequence these models have deficiencies  
in the representation of the motion of the grounding line which is a possible response  
to enhanced ice flux and upstream thinning. This is documented in the MIS-  
MIP and MIS-  
MIP-3d intercomparison projects (Pattyn et al., 2012, 2013).

*AIF* The Anisotropic Ice-Flow model is a 3-D ice-sheet model incorporating  
anisotropic ice flow and fully coupling dynamics and thermodynamics (Wang et al.,  
2012). It is a higher-order model with longitudinal and vertical shear stresses but cur-  
rently without an explicit representation of ice shelves. The model uses the finite differ-  
ence method to calculate ice-sheet geometry including isostatic bedrock adjustment,  
3-D distributions of shear and longitudinal strain rates, enhancement factors which ac-  
count for the effect of ice anisotropy, temperatures, horizontal and vertical velocities,  
shear and longitudinal stresses. The basal sliding is determined by Weertman's slid-  
ing law based on a cubic power relation of the basal shear stress. As the model lacks  
of ice shelves, the prescribed melt rates are applied to the ice-sheet perimeter grid-  
points only with a bed below sea level. The ice-sheet margin, which is equivalent to  
the grounding line in this model, moves freely within the model grid-points and the  
grounding line is detected by hydrostatic equilibrium (i.e. the floating condition) without  
sub-grid interpolation.

### Antarctic ice-discharge from SeaRISE response-functions

A. Levermann et al.

Title Page

Abstract

Introduction

Conclusions

References

Tables

Figures

◀

▶

◀

▶

Back

Close

Full Screen / Esc

Printer-friendly Version

Interactive Discussion



## Antarctic ice-discharge from SeaRISE response-functions

A. Levermann et al.

Title Page

Abstract

Introduction

Conclusions

References

Tables

Figures



Back

Close

Full Screen / Esc

Printer-friendly Version

Interactive Discussion

*Penn-State-3-D* The Penn State 3-D ice sheet model uses a hybrid combination of the scaled Shallow Ice (SIA) and Shallow Shelf (SSA) equations for shearing and longitudinal stretching flow respectively. The location of the grounding line is determined by simple flotation, with sub-grid interpolation as in (Gladstone et al., 2010). A parameterization relating ice velocity across the grounding line to local ice thickness is imposed as an internal boundary-layer condition, so that grounding-line migration is simulated reasonably well without the need for very high, i.e. of the order of 100 m, resolution (Schoof, 2007). Ocean melting below ice shelves and ice-shelf calving use simple parameterizations, along with a sub-grid parameterization at the floating-ice edge (Pollard and Deconto, 2009, 2012). The Penn-State-3-D model shows the best performance of grounding line motion within the MISMIP intercomparison compared to the other models applied here.

*PISM* The Parallel Ice Sheet Model ([www.pism-docs.org](http://www.pism-docs.org)) used here is based on version stable 0.4, which incorporates the Potsdam Parallel Ice Sheet Model (PISM-PIK) (Winkelmann et al., 2011; Martin et al., 2011). Ice flow is approximated by a hybrid scheme incorporating both the SIA and SSA approximations (Bueler and Brown, 2009). An enthalpy formulation (Aschwanden et al., 2012) is used for thermodynamics, and the model employs a physical stress-boundary condition to the shelfy-stream approximation at ice fronts, in combination with a sub-grid interpolation (Albrecht et al., 2011) and a kinematic first-order calving law (Levermann et al., 2012) at ice-shelf fronts. In PISM-PIK, the grounding line is not subject to any boundary conditions or flux corrections. Its position is determined from ice and bedrock topographies in each time step via the flotation criterion. The grounding line motion is thus influenced only indirectly by the velocities through the ice thickness evolution. Since the SSA (shallow shelf approximation) velocities are computed non-locally and simultaneously for the shelf and for the sheet, a continuous solution over the grounding line without singularities is ensured and buttressing effects are accounted for. The PISM model shows good performance of the grounding line motion within the MISMIP intercomparisons only at significantly higher resolution (1 km or finer) than applied here.



## Antarctic ice-discharge from SeaRISE response-functions

A. Levermann et al.

Title Page

Abstract

Introduction

Conclusions

References

Tables

Figures

⏪

⏩

◀

▶

Back

Close

Full Screen / Esc

Printer-friendly Version

Interactive Discussion

hardness depends, is obtained from a 1-D finite-element solution of the energy conservation equation at each node without direct representation of horizontal heat advection. This thermodynamic calculation includes vertical diffusion and advection, but neglects horizontal movement of heat. Also included is internal heat generation produced by shear with depth and sliding at the bed. Boundary conditions consist of specified surface temperature and basal geothermal gradient. If the calculated basal temperature exceeds the pressure melting point, the basal boundary condition is changed to a specified temperature, and a basal melt rate is calculated from the amount of latent heat of fusion that must be absorbed to maintain this specified temperature. Conversely, if the basal temperature drops below the pressure melting point where water is already present at the bed, a similar treatment allows for the calculation of a rate of basal freezing. A map-plane solution for conservation of water at the bed, whose source is the basal melt or freeze-on rate provided by the temperature solution, allows for movement of the basal water down the hydrostatic pressure gradient (Johnson and Fastook, 2002). Areas of basal sliding can be specified if known, or determined internally by the model as regions where lubricating basal water is present, produced either by melting in the thermodynamic calculation or by movement of water beneath the ice sheet down the hydrostatic gradient. Ice shelves are not modeled explicitly in UMISM. However, a thinning rate at the grounding line produced by longitudinal stresses is calculated from a parameterization of the thinning of a floating slab (Weertman, 1957). No sub-grid grounding line interpolation is applied.

Besides the probabilistic projections we apply the ice-sheet response functions to subsurface temperature projections from two different ocean models, namely the Bremerhaven Regional Ice Ocean Simulations (BRIOS) model and the Finite-Element Southern Ocean Model (FESOM).

*BRIOS* is a coupled ice–ocean model which resolves the Southern Ocean south of 50° S zonally at 1.5° and meridionally at 1.5° × cos  $\phi$ . The water column is variably divided into 24 terrain-following layers. The sea-ice component is a dynamic-thermodynamic snow/ice model with heat budgets for the upper and lower surface

## Antarctic ice-discharge from SeaRISE response-functions

A. Levermann et al.

Title Page

Abstract

Introduction

Conclusions

References

Tables

Figures

⏪

⏩

◀

▶

Back

Close

Full Screen / Esc

Printer-friendly Version

Interactive Discussion

layers (Parkinson and Washington, 1979) and a viscous-plastic rheology (Hibler III, 1979). BRIOS considers the ocean-ice shelf interaction underneath ten Antarctic ice shelves (Beckmann et al., 1999; Hellmer, 2004) with time-invariant thicknesses, assuming flux divergence and mass balance to be in dynamical equilibrium. The model has been successfully validated by the comparison with mooring and buoy observations regarding, e.g., Weddell gyre transport (Beckmann et al., 1999), sea ice thickness distribution and drift in Weddell and Amundsen seas (Timmermann et al., 2002a; Assmann et al., 2005) and sub-ice-shelf circulation (Timmermann et al., 2002b).

*FESOM* is a hydrostatic, primitive-equation ocean model with an unstructured grid that consists of triangles at the surface and tetrahedra in the ocean interior. It is based on the Finite Element model of the North Atlantic (Danilov et al., 2004, 2005) coupled to a dynamic-thermodynamic sea-ice model with a viscous-plastic rheology and evaluated in a global setup (Timmermann et al., 2009; Sidorenko et al., 2011). An ice-shelf component with a three-equation system for the computation of temperature and salinity in the boundary layer between ice and ocean and the melt rate at the ice shelf base (Hellmer et al., 1998) has been implemented. Turbulent fluxes of heat and salt are computed with coefficients depending on the friction velocity following Holland and Jenkins (1999). The present setup uses a hybrid vertical coordinate and a global mesh with a horizontal resolution between 30 and 40 km in the offshore Southern Ocean, which is refined to 10 km along the Antarctic coast, 7 km under the larger ice shelves in the Ross and Weddell Seas, and to 4 km under the small ice shelves in the Amundsen Sea.

Outside the Southern Ocean, resolution decreases to 50 km along the coasts and about 250–300 km in the vast basins of the Atlantic and Pacific Oceans, while on the other hand some of the narrow straits that are important to the global thermohaline circulation (e.g., Fram- and Denmark Straits, and the region between Iceland and Scotland) are represented with high resolution (Timmermann et al., 2012). Ice shelf draft, cavity geometry, and global ocean bathymetry have been derived from the RTopo-1

dataset (Timmermann et al., 2010) and thus consider data from many of the most recent surveys of the Antarctic continental shelf.

### 3 Deriving the response functions

In order to use the sensitivity experiments carried out within the SeaRISE project (Bindschadler et al., 2013), we assume that for the 21st century the temporal evolution of the ice-discharge can be expressed as

$$S(t) = \int_0^t d\tau R(t - \tau) m(\tau) \quad (1)$$

where  $S$  is the sea-level contribution from ice discharge,  $m$  is the forcing represented by the basal-melt rate and  $R$  is the ice-sheet response-function.  $t$  is time starting from a period prior to the beginning of a significant forcing. The responses function  $R$  can thus be understood as the response to a delta-peak forcing with magnitude one.

$$S_\delta(t) = \int_0^t d\tau R(t - \tau) \delta(\tau) = R(t) \quad (2)$$

We express ice-discharge throughout the paper in units of global mean sea-level equivalent. That means that in deriving the response functions we only diagnose ice loss above flotation that is relevant for sea level. As a simple consequence the response function is unitless. The basal ice-shelf melt signal as well as the ice-discharge signal used to derive the response functions are anomalies with respect to a baseline simulation under present-day boundary conditions (Bindschadler et al., 2013).

Linear response theory, as represented by Eq. (1), can only describe the response of a system up to a certain point in time; 100 yr is a relatively short period for the response

## Antarctic ice-discharge from SeaRISE response-functions

A. Levermann et al.

Title Page

Abstract

Introduction

Conclusions

References

Tables

Figures

⏪

⏩

◀

▶

Back

Close

Full Screen / Esc

Printer-friendly Version

Interactive Discussion





response to a step forcing is equivalent to the temporal integral of the response function  $R$  with  $t = 0$  being the time of the switch-on in forcing

$$S_{\text{sf}}(t) = \int_0^t d\tau R(t - \tau) \Delta m_0 \cdot \Theta(\tau) = \Delta m_0 \cdot \int_0^t d\tau R(\tau) \quad (3)$$

5 where  $\Theta(\tau)$  is the Heavyside function which is zero for negative  $\tau$  and one otherwise. We thus obtain the response function from

$$R(t) = \frac{1}{\Delta m_0} \cdot \frac{dS_{\text{sf}}}{dt}(t) \quad (4)$$

10 For the main results of this study we use the M2-experiment. While  $20 \text{ ma}^{-1}$  is a strong additional melting, it is within the range of potential future sub-shelf melt-rates as determined from the projected subsurface warming (see Fig. 5 and the empirical basal melt coefficients ( $7\text{--}16 \text{ ma}^{-1} \text{ K}^{-1}$ , Sect. 4.3). It provides a good signal-to-noise ratio in the experiments, i.e. the response of the ice-sheet to the forcing is dominated by the forcing and not by internal oscillations or long-term numerical drift. Since a linear relation  
 15 between response and forcing is assumed (Eq. 1) the forcing from which the response functions are derived should be similar to the forcing applied in the projections. Basal ice-shelf melt rates of the M1- ( $2 \text{ ma}^{-1}$ ) – and M3- ( $200 \text{ ma}^{-1}$ ) – experiments are either too low or too high and consequently yield slightly different results. Please note, however, that the explicit choice of the response function is of second-order with respect to  
 20 the uncertainty range of the sea-level projection. This can be seen when applying the response functions as obtained from the M1-experiments (Fig. 13). While the model- and basin-specific response functions may differ, the uncertainty range of the sea-level projections until 2100 (Fig. 13 lower panel) are very similar to the range obtained from the M2-experiment (Fig. 10). The reason for this similarity on the ranges is that most of  
 25 the uncertainty arises from the uncertainty in the external forcing, while the response

## Antarctic ice-discharge from SeaRISE response-functions

A. Levermann et al.

Title Page

Abstract

Introduction

Conclusions

References

Tables

Figures

⏪

⏩

◀

▶

Back

Close

Full Screen / Esc

Printer-friendly Version

Interactive Discussion



functions provide merely the magnitude of the continental scale response. See the appendix for more details.

The spatial distribution of the ice loss after 100 yr through additional basal ice-shelf melting illustrates the different dynamics of the ice-sheet models resulting from, for example, different representations of ice dynamics, surface mass balance, basal sliding parameterizations and numerical implementation (Fig. 3). Part of the individual responses result from the different representations of the basal ice-shelf melt. In the UMISM model basal melt was applied along the entire coastline which yields a particularly strong response in East Antarctica (Fig. 2). This is likely an overestimation of the ice loss compared to models with an explicit representation of ice shelves. On the other hand, coarse resolution ice-sheet models as used here cannot capture small ice shelves as they are present especially around East Antarctica. These models thus have a tendency to underestimate the fraction of the coastal ice that is afloat and thus sensitivity to changes in ocean temperature might be also underestimated (compare for example Martin et al., 2011, for the PISM model). While we will also provide projections using all five models, the main focus of the study are the three models with explicit representation of ice shelves (PennState-3-D, PISM and SICOPOLIS).

## 4 Probabilistic approach

We aim to estimate the sea level rise from Antarctic dynamic ice discharge driven by the global mean temperature evolution. In order to capture the climate uncertainty as well as the uncertainty in the oceanic response and the ice-sheet response, we follow a probabilistic approach that comprises four steps. (a) For each scenario, a climate forcing, i.e. global mean temperature evolution, that is consistent with the observed climate change and the range of climate sensitivity of 2–4.5° for a doubling of CO<sub>2</sub> is randomly selected, i.e. picked from the 600 global-mean-temperature time series. (b) The temperature evolution is translated into a time series of subsurface ocean temperature change by random selection from a set of scaling coefficients and the associated

## Antarctic ice-discharge from SeaRISE response-functions

A. Levermann et al.

Title Page

Abstract

Introduction

Conclusions

References

Tables

Figures

⏪

⏩

◀

▶

Back

Close

Full Screen / Esc

Printer-friendly Version

Interactive Discussion

## Antarctic ice-discharge from SeaRISE response-functions

A. Levermann et al.

Title Page

Abstract

Introduction

Conclusions

References

Tables

Figures

◀

▶

◀

▶

Back

Close

Full Screen / Esc

Printer-friendly Version

Interactive Discussion

time delay that correspond to one of the 19 CMIP-5 models. (c) The coefficient to translate the subsurface ocean temperature evolution to a sub-shelf melt rate is randomly drawn from the observation based interval  $7 \text{ ma}^{-1} \text{ K}^{-1}$  (Jenkins, 1991) to  $16 \text{ ma}^{-1} \text{ K}^{-1}$  (Payne et al., 2007). (d) To translate the melt rate to sea-level-relevant ice-loss from the associated ice-sheet basin we randomly pick one response function as derived in Sect. 2 (Fig. 2) and combine them with random selections of the forcing obtained from step (a)–(c).

The procedure is repeated 50 000 times.

### 4.1 Global mean temperature evolution

We here use the Representative Concentration Pathways (RCPs) (Moss et al., 2010; Meinshausen et al., 2011a). The range of possible changes in global mean temperature that result from each RCP is obtained by constraining the response of the emulator model MAGICC 6.0 (Meinshausen et al., 2011b) with the observed temperature record. This procedure has been used in several studies and aims to cover the possible global climate response to specific greenhouse-gas emission pathways (e.g. Meinshausen et al., 2009). Here we use a set of 600 time series of global mean temperature from the year 1850 to 2100 for each RCP that cover the full range of future global temperature changes as detailed in Schewe et al. (2011).

### 4.2 Subsurface oceanic temperatures from CMIP-5

We use the simulations of the recent Coupled Model Intercomparison (CMIP-5) and obtain a scaling relationship between the global mean temperature and the oceanic subsurface temperature for each model. This has been carried out for the CMIP-3 experiments by Winkelmann et al. (2012) and is repeated here for the more recent climate models of CMIP-5.

Our scaling approach is based on the assumption that anomalies of the ocean temperatures resulting from global warming scale with the respective anomalies in global





has already been discussed by Timmermann and Hellmer (2013). It therefore motivates the use of the broadest possible spectrum of climatic forcing in order to cover the high uncertainty from the choice of the global climate model.

## 6 Probabilistic projections of the Antarctic sea level contribution

### 6.1 Scaling coefficients for subsurface ocean temperatures

The scaling coefficients and the time delay determined from the 19 CMIP-5 coupled climate models are detailed in Tables 2–5. The high  $r^2$  values support the validity of the linear regression except for the IPSL model where also the slope between the two temperature signals is very low. We explicitly keep this model in order to include the possibility that almost no warming occurs underneath the ice-shelves.

Figure 5 shows the median and the 66 %- and 90 % probability ranges for the oceanic subsurface temperatures, denoted the *likely* and *very likely* range by the IPCC-AR4 (Solomon et al., 2007), as obtained from a random selection of global mean temperature pathways combined with a randomly selected scaling coefficient and the associated time delay  $\Delta t$  from Tables 2–5. Though physical reasons for a time delay between the surface and the subsurface temperatures exist, we find a high correlation also without applying a time delay. As the oceanic response of the coarse-resolution climate models applied here is likely to underestimate some small-scale transport processes (i.e. Hellmer et al., 2012), it is useful to also provide results without time delay to bracket the full range of response. The oceanic temperature time-series without time delay are provided as inlays in Fig. 5.

For comparison, Yin et al. (2011) assessed output from 19 AOGCMs under scenario A1B to determine how subsurface temperatures are projected to evolve around the ice sheets. They show decadal-mean warming of 0.4–0.7 °C and 0.4–0.9 °C around Antarctica (25th to 75th percentiles of ensemble, West and East respectively) between 1951–2000 and 2091–2100.

## Antarctic ice-discharge from SeaRISE response-functions

A. Levermann et al.

Title Page

Abstract

Introduction

Conclusions

References

Tables

Figures

⏪

⏩

◀

▶

Back

Close

Full Screen / Esc

Printer-friendly Version

Interactive Discussion



## 6.2 Projected sea-level contribution for the past (1992–2011)

Fig. 6 shows the uncertainty range of the sea-level projection as obtained from this procedure for the sea-level change between 1992 and 2011 together with the range for this quantity as obtained from observations (Shepherd et al., 2012). The bars in the upper panels show that the likely range (66 % percentile) of the models with explicit ice-shelf representations (PennState3-D, PISM and SICOPOLIS) are in good agreement with the observed range. The median (black dot) of each model is within the observed range. The middle panel shows that the time delay plays an important role. The likely range obtained from the models with explicit ice-shelf representation (denoted “Shelf-models” for simplicity) is almost identical with the observed range when the time delay is accounted for (dark red) while it reaches higher than the observed range without the time delay (dark blue). While we cannot claim that the ocean models nor the ice-sheet models are capable to simulate the specific (and largely unknown) events that resulted in the sea-level contribution from Antarctica between 1992 and 2011, the observed signal corresponds well with our estimated range.

## 6.3 Results for the different basins and different models

Fig. 7 shows the uncertainty range of the projected contribution from the different oceanic sectors comprising uncertainty in climate and ocean circulation. While the individual time series will differ from the non-probabilistic projections with the ocean models, FESOM and BRIOS, the order of magnitude of the range of the sea-level contribution is the same. For example, FESOM yields a particularly strong response in the Weddel sector when forced with the HadCM3 model (dashed lines in Fig. 4) and BRIOS a weak response when forced with ECHAM-5. The response of the models from the downscaled global simulations covers this range. While we find the largest median response in the Amundsen-Sea sector which forces the Pine-Island-Thwaites glaciers, the contributions of all sectors are relatively similar with a scatter of the median from 0.01 to 0.03 m (Fig. 8). Note, however, that the contributions from the different regions

### Antarctic ice-discharge from SeaRISE response-functions

A. Levermann et al.

Title Page

Abstract

Introduction

Conclusions

References

Tables

Figures



Back

Close

Full Screen / Esc

Printer-friendly Version

Interactive Discussion





subsurface ocean temperatures (Fig. 11 and Table 6). The results are summarized in Fig. 12. All distributions are significantly skewed towards high sea-level contributions. This skewness strongly influences the median of the distributions as well as the 66 %- and 90 %-ranges. Consequently the median is not the value with the highest probability. The large tails makes an estimate of the 90 %-range, i.e. the “very likely” range as denoted by the IPCC, very uncertain.

## 7 Conclusion and discussions

The aim of this study is to estimate the full range of potential sea level rise caused by future ice-discharge from Antarctica that can be induced by ocean warming within the 21st century. To this end we include the full range of climatic forcing climatic from models that yield practically no warming of the Southern Ocean subsurface (e.g. IPSL) to extreme cases with more than 2° of warming at the entrance of the ice-shelf cavities under the strongest warming scenario (Fig. 5).

The uncertainty ranges comprising climatic, oceanic and ice-dynamical uncertainty show a clear dependence on the global climate-change scenario (Table 6), especially for the tails of the distribution, e.g. the 90 % percentile. For the RCP-2.6 which was designed to result in a median increase in global mean temperature below 2° in most climate models, the 66 %-range of ice-loss is 0.02–0.14 m with a median of 0.07 m in units of sea-level rise. This range increases to 0.04–0.21 m for RCP-8.5 with a median contribution of 0.09 m. These results are based on the three models with explicit representation of ice-shelf dynamics. The strongest difference to the “ice-shelf models” arises in the UMISM model which applies melting along the entire coastline.

We have to note that the ice-sheet models as well as the climate models used here are coarse in horizontal model resolution. At this resolution the ice-sheet models are not able to simulate the benchmark behaviour of the MISMIP intercomparison projects (Pattyn et al., 2012, 2013). Two of the models used (PennState-3-D and PISM) are able to simulate the grounding line behaviour in accordance with analytic solutions or

## Antarctic ice-discharge from SeaRISE response-functions

A. Levermann et al.

Title Page

Abstract

Introduction

Conclusions

References

Tables

Figures

◀

▶

◀

▶

Back

Close

Full Screen / Esc

Printer-friendly Version

Interactive Discussion





order to be able to model the entire continent, the main uncertainty in this study arises from the uncertainty in forcing not from the ice-sheet model.

The linear response approach puts further limits to our results. A significant response time of the sea-level-relevant ice-flow to basal ice-shelf melting will be multi-decadal or longer which justifies the use of a linear response function to represent the full non-linear dynamics. A clear short-coming is, however, that the method is not capable of capturing self-amplification processes within the ice. As a consequence an irreversible grounding line motion will be captured only when it is forced and not if it is merely triggered by the forcing and then self-amplifies. Thus, if the ice loss due to an instability is faster than due to the external forcing, then this additional ice loss will not be captured properly by the linear response theory. This is particularly relevant for weak forcing scenarios in which an instability might be triggered but the directly forced ice loss is weak. For strong forcing scenarios like the RCP-8.5 the forcing is likely to dominate the dynamics.

Changes in the geometry of the ice-shelf cavity and salinity changes due to melt water cannot be accounted for in a systematic way here. While the three ice models with ice shelf representation within the limitation of their resolution incorporate dynamic shelf evolution, the geometry changes cannot feed back to the ocean circulation in our linear response approach. The computation of the basal ice-shelf melt anomalies from the temperature anomalies is simplified as it excludes salinity changes. However, the simplification well approximates the dominating dynamics as the effect of salinity anomalies is small (Payne et al., 2007). To account for the feedbacks between ice thickness and salinity changes due to melt water and the ocean circulation, interactive coupling of ice shelves models and global climate models is needed. As dynamic ice shelf models are not implemented in the CMIP-5 climate models applied, the feedbacks cannot be reliably projected within the probabilistic approach taken here. We do not account for melt patterns underneath the ice-shelves as basal melt rates are applied uniformly. While it has been shown that the melting distribution matters for the ice-sheet response (Walker et al., 2008; Gagliardini et al., 2010), it is beyond the scope of this

**Antarctic  
ice-discharge from  
SeaRISE  
response-functions**

A. Levermann et al.

Title Page

Abstract

Introduction

Conclusions

References

Tables

Figures



Back

Close

Full Screen / Esc

Printer-friendly Version

Interactive Discussion



study as a dynamic ocean model is not applied. The melt coefficients applied here were derived for as as an ice shelf average and new uncertainty would be introduced with a spatially dependent melt coefficient.

As discussed above, a time lag between the oceanic temperature change and the change in global mean temperature is physically reasonable and applied in our projections. However, the correlation between surface warming and subsurface temperature change improves only marginally when introducing the time lag and it is not clear whether small scale processes may accelerate the heat transport at finer resolution (Hellmer et al., 2012). It is thus worthwhile to consider the ice loss without a time lag (Fig. 10b). If the basal ice-shelf melt rates are applied immediately the 66%-range of the sea level contribution increases from 0.04–0.21 m to 0.07–0.28 m for RCP-8.5. The simulations with the high-resolution finite-element ocean model FESOM and the regional ocean model BRIOS (Fig. 4) illustrate that abrupt ocean circulation changes can have strong influence on the basal melt rates (Hellmer et al., 2012). The comparably coarse-resolution ocean components of the CMIP-5 global climate models are unlikely to resolve such small scale changes. Estimates on as presented here will thus be dominated by basin-scale temperature changes of the interior ocean.

The probabilistic approach applied here assumes a certain interdependence of the different uncertainties. The global climatic signal is selected independently from the oceanic scaling coefficient. However the range of scaling coefficients is derived from the correlation within the different CMIP-5 models. The ice-sheet uncertainty is again independent of the other two components. While there are other methods to combine the uncertainties, we find no clear way of judging which method is superior.

The ice-loss computed here is a response entirely to enhanced basal ice-shelf melting. There are other potential changes in the boundary conditions and dynamics of the ice-sheet such as softening through ice warming and enhanced basal sliding as well as abrupt ice-shelf disintegration (not induced by basal ice-shelf melting) which might play a significant role for future ice-discharge from Antarctica.

## Antarctic ice-discharge from SeaRISE response-functions

A. Levermann et al.

Title Page

Abstract

Introduction

Conclusions

References

Tables

Figures



Back

Close

Full Screen / Esc

Printer-friendly Version

Interactive Discussion

The method presented here can easily be applied to other ice-sheet models with improved dynamical representation as they become available. This study is merely a first step towards comprising the full range of forcing uncertainty into an estimate of the future sea-level contribution from Antarctica.

## 5 Appendix A

### Linear response function derived from SeaRISE M1-experiment

Figure 13 shows the response functions as obtained from the M1 experiment with  $2 \text{ ma}^{-1}$  of additional basal ice-shelf melting. Comparison with Fig. 2 shows significant differences between the response functions obtained from the M1- and M2-experiments.

The lower panels of Fig. 13 show, however that the uncertainty range of the sea-level projection is very similar to the projections obtained with the M2-experiment (Fig. 10). This illustrates the fact that the uncertainty range is dominated by the external forcing of the ice-sheets, while the response functions provide merely the magnitude of the ice-sheet response to the forcing. For the ultimate uncertainty range it is herein not crucial whether the response function of one specific model is different for the M1 and the M2 experiments as long as the range of responses spanned by all three models is similar. This supports the use of the probabilistic approach taken in this study.

*Acknowledgements.* RW and MAM were funded by the German federal ministry of education and research (BMBF grant 01LP1171A). MM was funded by the Deutsche Bundestiftung Umwelt. RG and TS were supported by a Grant-in-Aid for Scientific Research A (No. 22244058) from the Japan Society for the Promotion of Science (JSPS). SN, RAB, and WLW were supported by the NASA Cryospheric Science program (Grants 281945.02.53.02.19 and 281945.02.53.02.20). KF was by the German Federal Ministry for the Environment, Nature Conservation and Nuclear Safety (11\_II\_093\_Global\_A\_SIDS and LDCs). HHH, AJP and RT were supported by the ice2sea programme from the European Union 7th Framework Programme, grant no. 226375.

## Antarctic ice-discharge from SeaRISE response-functions

A. Levermann et al.

Title Page

Abstract

Introduction

Conclusions

References

Tables

Figures



Back

Close

Full Screen / Esc

Printer-friendly Version

Interactive Discussion



## References

- Albrecht, T., Martin, M., Haseloff, M., Winkelmann, R., and Levermann, A.: Parameterization for subgrid-scale motion of ice-shelf calving fronts, *The Cryosphere*, 5, 35–44, doi:10.5194/tc-5-35-2011, 2011. 1123
- 5 Aschwanden, A., Bueler, E., Khroulev, C., and Blatter, H.: An enthalpy formulation for glaciers and ice sheets, *J. Glaciol.*, 58, 441–457, doi:10.3189/2012JoG11J088, 2012. 1123
- Assmann, K. M., Hellmer, H. H., and Jacobs, S. S.: Amundsen Sea ice production and transport, *J. Geophys. Res.*, 110, 311–337, 2005. 1126
- Bamber, J. L., Riva, R. E. M., Vermeersen, B. L. A., and LeBrocq, A. M.: Reassessment of the potential sea-level rise from a collapse of the West Antarctic Ice Sheet, *Science*, 324, 901–903, doi:10.1126/science.1169335, 2009. 1120
- 10 Beckmann, A., Hellmer, H. H., and Timmermann, R.: A numerical model of the Weddell Sea: large-scale circulation and water mass distribution, *Geophys. Res. Lett.*, 104, 23375–23391, 1999. 1126
- 15 Bindschadler, R. A., Nowicki, S., Abe-Ouchi, A., Aschwanden, A., Choi, H., Fastook, J., Granzow, G., Greve, R., Gutowski, G., Herzfeld, U., Jackson, C., Johnson, J., Khroulev, C., Levermann, A., Lipscomb, W. H., Martin, M., Morlighem, M., Parizek, B., Pollard, D., Price, S. F., Ren, D., Saito, F., Sato, T., Seddik, H., Seroussi, H., Takahashi, K., Walker, R., and Wang, W. L.: Ice-sheet model sensitivities to environmental forcing and their use in projecting future sea level (The SeaRISE Project), *J. Glaciol.*, 59, 195–224, doi:10.3189/2013JoG12J125, 2013. 1121, 1122, 1127, 1128
- 20 Bueler, E. and Brown, J.: The shallow shelf approximation as a sliding law in a thermomechanically coupled ice sheet model, *J. Geophys. Res.*, 114, F03008, doi:10.1029/2008JF001179, 2009. 1123
- 25 Danilov, S., Kivman, G., and Schröter, J.: A finite element ocean model: principles and evaluation, *Ocean Model.*, 6, 125–150, 2004. 1126
- Danilov, S., Kivman, G., and Schröter, J.: Evaluation of an eddy-permitting finite-element ocean model in the North Atlantic, *Ocean Model.*, 10, 35–49, 2005. 1126
- 30 Fastook, J. L.: A map-plane finite-element program for ice sheet reconstruction: a steady-state calibration with Antarctica and a reconstruction of the Laurentide Ice Sheet for 18,000 BP, in: *Computer Assisted Analysis and Modeling on the IBM 3090*, edited by: Brown, H. U., IBM Scientific and Technical Computing Dept., White Plains, NY, 1990. 1124

### Antarctic ice-discharge from SeaRISE response-functions

A. Levermann et al.

Title Page

Abstract

Introduction

Conclusions

References

Tables

Figures



Back

Close

Full Screen / Esc

Printer-friendly Version

Interactive Discussion



**Antarctic  
ice-discharge from  
SeaRISE  
response-functions**

A. Levermann et al.

Title Page

Abstract

Introduction

Conclusions

References

Tables

Figures



Back

Close

Full Screen / Esc

Printer-friendly Version

Interactive Discussion

- Fastook, J. L.: The finite-element method for solving conservation equations in glaciology, *Computational Science and Engineering*, 1, 55–67, 1993. 1124
- Fastook, J. L. and Chapman, J.: A map plane finite-element model: three modeling experiments, *J. Glaciol.*, 35, 48–52, 1989. 1124
- 5 Fastook, J. L. and Hughes, T. J.: Changing ice loads on the Earth's surface during the last glacial cycle, in: *Glacial Isostasy, Sea-Level and Mantle Rheology, Series C: Mathematical and Physical Sciences*, Vol. 334, edited by: Sabadini, R., Lambeck, K., and Boschi, E., Kluwer Academic Publishers, Dordrecht/Boston/London, 1990. 1124
- Fastook, J. L. and Prentice, M.: A finite-element model of Antarctica: Sensitivity test for meteorological mass balance relationship, *J. Glaciol.*, 40, 167–175, 1994. 1124
- 10 Fastook, J. L., Head, J. W., Forget, F., Madeleine, J.-B., and Marchant, D. R.: Evidence for Amazonian northern mid-latitude regional glacial landsystems on Mars: glacial flow models using GCM-driven climate results and comparisons to geological observations, *Icarus*, 216, 23–39, 2011. 1124
- 15 Fastook, J. L., Head, J. W., Marchant, D. R., Forget, F., and Madeleine, J.-B.: Early Mars climate near the Noachian–Hesperian Boundary: independent evidence for cold conditions from basal melting of the south polar ice sheet (Dorsa Argentea Formation) and implications for valley network formation, *Icarus*, 219, 25–40, 2012. 1124
- Gagliardini, O., Durand, G., Zwinger, T., Hindmarsh, R. C. A., and Le Meur, E.: Coupling of ice-shelf melting and buttressing is a key process in ice-sheets dynamics, *Geophys. Res. Lett.*, 37, L14501, doi:10.1029/2010GL043334, 2010. 1139
- 20 Gladstone, R. M., Payne, A. J., and Cornford, S. L.: Parameterising the grounding line in flow-line ice sheet models, *The Cryosphere*, 4, 605–619, doi:10.5194/tc-4-605-2010, 2010. 1123
- Good, P., Gregory, J. M., and Lowe, J. A.: A step-response simple climate model to reconstruct and interpret AOGCM projections, *Geophys. Res. Lett.*, 38, 1703, doi:10.1029/2010GL045208, 2011. 1122
- 25 Greve, R.: *Thermomechanisches Verhalten polythermer Eisschilde – Theorie, Analytik, Numerik*, Ph.D. thesis, Department of Mechanics, Darmstadt University of Technology, Germany, *Berichte aus der Geowissenschaft*, Shaker Verlag, Aachen, Germany, 1995. 1124
- 30 Greve, R.: Application of a polythermal three-dimensional ice sheet model to the Greenland ice sheet: response to steady-state and transient climate scenarios, *J. Climate*, 10, 901–918, doi:10.1175/1520-0442(1997)010<0901:AOAPTD>2.0.CO;2, 1997. 1124

## Antarctic ice-discharge from SeaRISE response-functions

A. Levermann et al.

Title Page

Abstract

Introduction

Conclusions

References

Tables

Figures

◀

▶

◀

▶

Back

Close

Full Screen / Esc

Printer-friendly Version

Interactive Discussion

- Greve, R.: Relation of measured basal temperatures and the spatial distribution of the geothermal heat flux for the Greenland ice sheet, *Ann. Glaciol.*, 42, 424–432, doi:10.3189/172756405781812510, 2005. 1124
- Greve, R. and Blatter, H. (Eds.): *Dynamics of Ice Sheets and Glaciers*, Springer, Berlin & Heidelberg, Germany, 2009. 1124
- Hellmer, H., Kauker, F., Timmermann, R., Determann, J., and Rae, J.: Twenty-first-century warming of a large Antarctic ice-shelf cavity by a redirected coastal current, *Nature*, 485, 225–228, 2012. 1133, 1134, 1140
- Hellmer, H. H.: Impact of Antarctic ice shelf basal melting on sea ice and deep ocean properties, *Geophys. Res. Lett.*, 31, L10307, doi:10.1029/2004GL019506, 2004. 1126
- Hellmer, H. H. and Olbers, D. J.: A two-dimensional model for the thermohaline circulation under an ice shelf, *Antarct. Sci.*, 1, 325–336, 1989. 1132
- Hellmer, H. H., Jacobs, S. S., and Jenkins, A.: Oceanic erosion of a floating Antarctic glacier in the Amundsen Sea, in: *Ocean, Ice and Atmosphere: Interactions at Antarctic Continental Margin*, edited by: Jacobs, S. S. and Weiss, R., vol. 75 of *Antarctic Research Series*, American Geophysical Union, Washington DC, 83–100, 1998. 1126
- Hibler III, W. D.: A dynamic-thermodynamic sea ice model, *J. Phys. Oceanogr.*, 9, 815–846, 1979. 1126
- Holland, D. M. and Jenkins, A.: Modeling thermodynamic ice–ocean interactions at the base of an ice shelf, *J. Climate*, 29, 1787–1800, 1999. 1126
- Holland, P. R., Jenkins, A., and Holland, D. M.: The response of ice shelf basal melting to variations in ocean temperature, *J. Climate*, 21, 2558–2572, 2008. 1132
- Hutter, K. (Ed.): *Theoretical glaciology*, D. Reidel Publishing Company/Terra Scientific Publishing Company, Tokyo, 1983. 1124
- Huybrechts, P., Goelzer, H., Janssens, I., Driesschaert, E., Fichfet, T., Goosse, H., and Loutre, M.-F.: Response of the Greenland and Antarctic ice sheets to multi-millennial greenhouse warming in the Earth System Model of intermediate complexity LOVECLIM, *Surv. Geophys.*, 32, 397–416, 2011. 1120
- Jenkins, A.: Ice shelf basal melting: implications of a simple mathematical model, *Tech. Rep. FRISP Rep. 5*, Geophysical Institute Bergen, Bergen, Norway, 1991. 1131, 1132
- Johnson, J. and Fastook, J. L.: Northern Hemisphere glaciation and its sensitivity to basal melt water, *Quaternary Int.*, 95–96, 65–74, 2002. 1125

## Antarctic ice-discharge from SeaRISE response-functions

A. Levermann et al.

[Title Page](#)
[Abstract](#)
[Introduction](#)
[Conclusions](#)
[References](#)
[Tables](#)
[Figures](#)
[◀](#)
[▶](#)
[◀](#)
[▶](#)
[Back](#)
[Close](#)
[Full Screen / Esc](#)
[Printer-friendly Version](#)
[Interactive Discussion](#)


Le Brocq, A. M., Payne, A. J., and Vieli, A.: An improved Antarctic dataset for high resolution numerical ice sheet models (ALBMAP v1), *Earth Syst. Sci. Data*, 2, 247–260, doi:10.5194/essd-2-247-2010, 2010. 1150, 1156

Le Meur, E. and Huybrechts, P.: A comparison of different ways of dealing with isostasy: examples from modelling the Antarctic ice sheet during the last glacial cycle, *Ann. Glaciol.*, 23, 309–317, 1996. 1124

Levermann, A., Albrecht, T., Winkelmann, R., Martin, M. A., Haseloff, M., and Joughin, I.: Kinematic first-order calving law implies potential for abrupt ice-shelf retreat, *The Cryosphere*, 6, 273–286, doi:10.5194/tc-6-273-2012, 2012. 1123

Levermann, A., Clark, P. U., Marzeion, B., Milnee, G. A., Pollard, D., Radic, V., and Robinson, A.: The multimillennial sea-level commitment of global warming, *P. Natl. Acad. Sci. USA*, 110, 13745–13750, doi:10.1073/pnas.1219414110, 2013. 1120

MacAyeal, D. R.: Large-scale ice flow over a viscous basal sediment – theory and application to ice stream B, Antarctica, *J. Geophys. Res.*, 94, 4071–4087, 1989. 1124

Martin, M. A., Winkelmann, R., Haseloff, M., Albrecht, T., Bueler, E., Khroulev, C., and Levermann, A.: The Potsdam Parallel Ice Sheet Model (PISM-PIK) – Part 2: Dynamic equilibrium simulation of the Antarctic ice sheet, *The Cryosphere*, 5, 727–740, doi:10.5194/tc-5-727-2011, 2011. 1123, 1130

Meinshausen, M., Meinshausen, N., Hare, W., Raper, S. C. B., Frieler, K., Knutti, R., Frame, D. J., and Allen, M. R.: Greenhouse-gas emission targets for limiting global warming to 2°C, *Nature*, 458, 1158–1162, 2009. 1131

Meinshausen, M., Smith, S., Calvin, K., Daniel, J., Kainuma, M., Lamarque, J.-F., Matsumoto, K., Montzka, S., Raper, S., Riahi, K., Thomson, A., Velders, G., and van Vuuren, D. P.: The RCP greenhouse gas concentrations and their extensions from 1765 to 2300, *Climatic Change*, 109, 213–241, doi:10.1007/s10584-011-0156-z, 2011a. 1121, 1131

Meinshausen, M., Raper, S. C. B., and Wigley, T. M. L.: Emulating coupled atmosphere-ocean and carbon cycle models with a simpler model, *MAGICC6 – Part 1: Model description and calibration*, *Atmos. Chem. Phys.*, 11, 1417–1456, doi:10.5194/acp-11-1417-2011, 2011b. 1131

Mitrovica, J. X., Gomez, N., and Clark, P. U.: The sea-level fingerprint of West Antarctic collapse, *Science*, 323, 753–753, 2009. 1120

Morland, L. W.: Thermomechanical balances of ice sheet flows, *Geophys. Astro. Fluid*, 29, 237–266, 1984. 1124

## Antarctic ice-discharge from SeaRISE response-functions

A. Levermann et al.

[Title Page](#)
[Abstract](#)
[Introduction](#)
[Conclusions](#)
[References](#)
[Tables](#)
[Figures](#)
[◀](#)
[▶](#)
[◀](#)
[▶](#)
[Back](#)
[Close](#)
[Full Screen / Esc](#)
[Printer-friendly Version](#)
[Interactive Discussion](#)

Morland, L. W.: Unconfined ice-shelf flow, in: Dynamics of the West Antarctic Ice Sheet, edited by: Van der Veen, C. J. and Oerlemans, J., Cambridge University Press, Cambridge, UK, 117–140, 1987. 1124

Moss, R. H., Edmonds, J. A., Hibbard, K. A., Manning, M. R., Rose, S. K., van Vuuren, D. P., Carter, T. R., Emori, S., Kainuma, M., Kram, T., Meehl, G. A., Mitchell, J. F. B., Nakicenovic, N., Riahi, K., Smith, S. J., Stouffer, R. J., Thomson, A. M., Weyant, J. P., and Wilbanks, T. J.: The next generation of scenarios for climate change research and assessment, *Nature*, 463, 747–756, 2010. 1121, 1131

Nowicki, S., Bindschadler, R. A., Abe-Ouchi, A., Aschwanden, A., Bueller, E., Choi, H., Fastook, J., Granzow, G., Greve, R., Gutowski, G., Herzfeld, U. C., Jackson, C., Johnson, J., Khroulev, C., Larour, E., Levermann, A., Lipscomb, W. H., Martin, M. A., Morlighem, M., Parizek, B. R., Pollard, D., Price, S. F., Ren, D., Rignot, E., Saito, F., Sato, T., Seddik, H., Seroussi, H., Takahashi, K., Walker, R., and Wang, W. L.: Insights into spatial sensitivities of ice mass response to environmental change from the SeaRISE ice sheet modeling project I: Antarctica, *J. Geophys. Res.-Earth*, 118, 1002–1024, doi:10.1002/jgrf.20081, 2013a. 1121, 1158

Nowicki, S., Bindschadler, R. A., Abe-Ouchi, A., Aschwanden, A., Bueller, E., Choi, H., Fastook, J., Granzow, G., Greve, R., Gutowski, G., Herzfeld, U. C., Jackson, C., Johnson, J., Khroulev, C., Larour, E., Levermann, A., Lipscomb, W. H., Martin, M. A., Morlighem, M., Parizek, B. R., Pollard, D., Price, S. F., Ren, D., Rignot, E., Saito, F., Sato, T., Seddik, H., Seroussi, H., Takahashi, K., Walker, R., and Wang, W. L.: Insights into spatial sensitivities of ice mass response to environmental change from the SeaRISE ice sheet modeling project II: Greenland, *J. Geophys. Res.-Earth*, 118, 1025–1044, doi:10.1002/jgrf.20076, 2013b. 1121

Parkinson, C. L. and Washington, W. M.: A large-scale numerical model of sea ice, *J. Geophys. Res.*, 84, 311–337, 1979. 1126

Pattyn, F., Schoof, C., Perichon, L., Hindmarsh, R. C. A., Bueller, E., de Fleurian, B., Durand, G., Gagliardini, O., Gladstone, R., Goldberg, D., Gudmundsson, G. H., Huybrechts, P., Lee, V., Nick, F. M., Payne, A. J., Pollard, D., Rybak, O., Saito, F., and Vieli, A.: Results of the Marine Ice Sheet Model Intercomparison Project, MISMP, *The Cryosphere*, 6, 573–588, doi:10.5194/tc-6-573-2012, 2012. 1122, 1124

Pattyn, F., Perichon, L., Durand, G., Favier, L., Gagliardini, O., Hindmarsh, R., Zwinger, T., Albrecht, T., Cornford, S. L., Docquier, D., Fuerst, J. J., Goldberg, D., Gudmundsson, G., Humbert, A., Huetten, M., Huybrechts, P., Jouvett, G., Kleiner, T., Larour, E.,

## Antarctic ice-discharge from SeaRISE response-functions

A. Levermann et al.

Title Page

Abstract

Introduction

Conclusions

References

Tables

Figures

◀

▶

◀

▶

Back

Close

Full Screen / Esc

Printer-friendly Version

Interactive Discussion

Martin, D., Morlighem, M., Payne, T., Pollard, D., Rueckamp, M., Rybak, O., Seroussi, H., Thoma, M., and Wilkens, N.: Grounding-line migration in plan-view marine ice-sheet models: results of the ice2sea MISMIP3d intercomparison, *J. Glaciol.*, 59, 410–422, doi:10.3189/2013JoG12J129, 2013. 1122

5 Payne, A. J., Holland, P. R., Shepherd, A. P., Rutt, I. C., Jenkins, A., and Joughin, I.: Numerical modeling of ocean-ice interactions under Pine Island Bay's ice shelf, *J. Geophys. Res.*, 112, C10019, doi:10.1029/2006JC003733, 2007. 1131, 1132, 1139

Pollard, D. and Deconto, R. M.: Modelling West Antarctic ice sheet growth and collapse through the past five million years, *Nature*, 458, 329–332, 2009. 1123

10 Pollard, D. and DeConto, R. M.: Description of a hybrid ice sheet-shelf model, and application to Antarctica, *Geosci. Model Dev.*, 5, 1273–1295, doi:10.5194/gmd-5-1273-2012, 2012. 1123

Sato, T.: Dynamics of the Antarctic ice sheet with coupled ice shelves, Ph.D. thesis, Graduate School of Environmental Science, Hokkaido University, Sapporo, Japan, available at: <http://tinyurl.com/GISRG42> (last access: 12 December 2013), 2012. 1124

15 Sato, T. and Greve, R.: Sensitivity experiments for the Antarctic ice sheet with varied sub-ice-shelf melting rates, *Ann. Glaciol.*, 53, 221–228, doi:10.3189/2012AoG60A042, 2012. 1124

Schewe, J., Levermann, A., and Meinshausen, M.: Climate change under a scenario near 1.5 °C of global warming: monsoon intensification, ocean warming and steric sea level rise, *Earth Syst. Dynam.*, 2, 25–35, doi:10.5194/esd-2-25-2011, 2011. 1131

20 Schoof, C.: Ice sheet grounding line dynamics: steady states, stability, and hysteresis, *J. Geophys. Res.-Earth*, 112, F03S28, doi:10.1029/2006JF000664, 2007. 1123

Shepherd, A., Ivins, E. R., Geruo, A., Barletta, V. R., Bentley, M. J., Bettadpur, S., Briggs, K. H., Bromwich, D. H., Forsberg, R., Galin, N., Horwath, M., Jacobs, S., Joughin, I., King, M. A., Lenaerts, J. T. M., Li, J., Ligtenberg, S. R. M., Luckman, A., Luthcke, S. B., McMillan, M., Meister, R., Milne, G., Mougnot, J., Muir, A., Nicolas, J. P., Paden, J., Payne, A. J., Pritchard, H., Rignot, E., Rott, H., Sorensen, L. S., Scambos, T. A., Scheuchl, B., Schrama, E. J. O., Smith, B., Sundal, A. V., van Angelen, J. H., van de Berg, W. J., van den Broeke, M. R., Vaughan, D. G., Velicogna, I., Wahr, J., Whitehouse, P. L., Wingham, D. J., Yi, D., Young, D., and Zwally, H. J.: A reconciled estimate of ice-sheet mass balance, *Science*, 338, 1183–1189, doi:10.1126/science.1228102, 2012. 1135, 1161

30 Sidorenko, D., Wang, Q., Danilov, S., and Schröter, J.: FESOM under coordinated Ocean-ice Reference Experiment forcing, *Ocean Dynam.*, doi:10.1007/s10236-011-0406-7, 2011. 1126



**Antarctic  
ice-discharge from  
SeaRISE  
response-functions**

A. Levermann et al.

Title Page

Abstract

Introduction

Conclusions

References

Tables

Figures

⏪

⏩

◀

▶

Back

Close

Full Screen / Esc

Printer-friendly Version

Interactive Discussion

- Walker, R. T., Dupont, T. K., Parizek, B. R., and Alley, R. B.: Effects of basal-melting distribution on the retreat of ice-shelf grounding lines, *Geophys. Res. Lett.*, 35, L17503, doi:10.1029/2008GL034947, 2008. 1139
- Wang, W., Li, J., and Zwally, H. J.: Dynamic inland propagation of thinning due to ice loss at the margins of the Greenland ice sheet, *J. Glaciol.*, 58, 734–740, doi:10.3189/2012JoG11J187, 2012. 1122
- Weertman, J.: Deformation of floating ice shelves, *J. Glaciol.*, 3, 38–42, 1957. 1125
- Winkelmann, R. and Levermann, A.: Linear response functions to project contributions to future sea level, *Clim. Dynam.*, 40, 2579–2588, doi:10.1007/s00382-012-1471-4, 2013. 1128
- Winkelmann, R., Martin, M. A., Haseloff, M., Albrecht, T., Bueller, E., Khroulev, C., and Levermann, A.: The Potsdam Parallel Ice Sheet Model (PISM-PIK) – Part 1: Model description, *The Cryosphere*, 5, 715–726, doi:10.5194/tc-5-715-2011, 2011. 1123
- Winkelmann, R., Levermann, A., Frieler, K., and Martin, M. A.: Uncertainty in future solid ice discharge from Antarctica, *The Cryosphere Discuss.*, 6, 673–714, doi:10.5194/tcd-6-673-2012, 2012. 1131
- Yin, J., Overpeck, J., Griffies, S., Hu, A., Russell, J., and Stouffer, R. J.: Different magnitudes of projected subsurface ocean warming around Greenland and Antarctica, *Nature Climate Change*, 4, 524–528, 2011. 1134

**Antarctic  
ice-discharge from  
SeaRISE  
response-functions**

A. Levermann et al.

Title Page

Abstract

Introduction

Conclusions

References

Tables

Figures

◀

▶

◀

▶

Back

Close

Full Screen / Esc

Printer-friendly Version

Interactive Discussion

**Table 1.** Mean depth of ice shelves in the different regions denoted in Fig. 1 as computed from (Le Brocq et al., 2010). Oceanic temperature anomalies were averaged vertically over a 100 m range around these depth.

Region	Depth [m]
Amundsen Sea	305
Ross Sea	312
Weddell Sea	420
East Antarctica	369

## Antarctic ice-discharge from SeaRISE response-functions

A. Levermann et al.

[Title Page](#)
[Abstract](#)
[Introduction](#)
[Conclusions](#)
[References](#)
[Tables](#)
[Figures](#)
[⏪](#)
[⏩](#)
[◀](#)
[▶](#)
[Back](#)
[Close](#)
[Full Screen / Esc](#)
[Printer-friendly Version](#)
[Interactive Discussion](#)

**Table 2.** Amundsen-Sea sector: scaling coefficients and time delay  $\Delta t$  between increase in global mean temperature and subsurface ocean temperature anomaly.

Model	Coeff. without $\Delta t$	$r^2$	$\Delta t$ [yr]	Coeff. with $\Delta t$	$r^2$
ACCESS1-0	0.17	0.86	0	0.17	0.86
ACCESS1-3	0.30	0.94	0	0.30	0.94
BNU-ESM	0.37	0.88	30	0.56	0.92
CanESM2	0.15	0.83	30	0.24	0.88
CCSM4	0.22	0.89	0	0.22	0.89
CESM1-BGC	0.19	0.92	0	0.19	0.92
CESM1-CAM5	0.12	0.92	0	0.12	0.92
CSIRO-Mk3-6-0	0.16	0.79	30	0.28	0.83
FGOALS-s2	0.24	0.90	55	0.54	0.93
GFDL-CM3	0.26	0.81	35	0.49	0.85
HadGEM2-ES	0.23	0.70	0	0.23	0.70
INMCM4	0.67	0.90	0	0.67	0.90
IPSL-CM5A-MR	0.07	0.22	90	0.44	0.45
MIROC-ESM-CHEM	0.12	0.74	5	0.13	0.75
MIROC-ESM	0.11	0.55	60	0.35	0.61
MPI-ESM-LR	0.27	0.80	5	0.29	0.82
MRI-CGCM3	0.00	0.02	85	-0.07	0.04
NorESM1-M	0.30	0.94	0	0.30	0.94
NorESM1-ME	0.31	0.89	0	0.31	0.89

## Antarctic ice-discharge from SeaRISE response-functions

A. Levermann et al.

[Title Page](#)
[Abstract](#)
[Introduction](#)
[Conclusions](#)
[References](#)
[Tables](#)
[Figures](#)
[⏪](#)
[⏩](#)
[◀](#)
[▶](#)
[Back](#)
[Close](#)
[Full Screen / Esc](#)
[Printer-friendly Version](#)
[Interactive Discussion](#)

**Table 3.** Weddell sector: scaling coefficients and time delay  $\Delta t$  between increase in global mean temperature and subsurface ocean temperature anomaly.

Model	Coeff. without $\Delta t$	$r^2$	$\Delta t$ [yr]	Coeff. with $\Delta t$	$r^2$
ACCESS1-0	0.07	0.73	35	0.14	0.80
ACCESS1-3	0.07	0.73	35	0.15	0.81
BNU-ESM	0.37	0.89	0	0.37	0.89
CanESM2	0.11	0.82	55	0.31	0.91
CCSM4	0.37	0.95	20	0.49	0.96
CESM1-BGC	0.37	0.95	25	0.53	0.96
CESM1-CAM5	0.23	0.79	50	0.63	0.88
CSIRO-Mk3-6-0	0.19	0.80	55	0.60	0.90
FGOALS-s2	0.09	0.73	85	0.39	0.86
GFDL-CM3	0.11	0.55	60	0.31	0.62
HadGEM2-ES	0.31	0.92	0	0.31	0.92
INMCM4	0.26	0.83	10	0.30	0.83
IPSL-CM5A-MR	-0.02	0.00	85	-0.06	0.03
MIROC-ESM-CHEM	0.07	0.50	65	0.32	0.77
MIROC-ESM	0.03	0.27	65	0.18	0.59
MPI-ESM-LR	0.08	0.65	85	0.41	0.70
MRI-CGCM3	0.21	0.63	40	0.47	0.83
NorESM1-M	0.26	0.90	5	0.28	0.92
NorESM1-ME	0.25	0.85	50	0.64	0.92

## Antarctic ice-discharge from SeaRISE response-functions

A. Levermann et al.

Title Page

Abstract

Introduction

Conclusions

References

Tables

Figures

◀

▶

◀

▶

Back

Close

Full Screen / Esc

Printer-friendly Version

Interactive Discussion

**Table 4.** Ross-Sea sector: scaling coefficients and time delay  $\Delta t$  between increase in global mean temperature and subsurface ocean temperature anomaly.

Model	Coeff. without $\Delta t$	$r^2$	$\Delta t$ [yr]	Coeff. with $\Delta t$	$r^2$
ACCESS1-0	0.18	0.77	20	0.26	0.79
ACCESS1-3	0.09	0.76	15	0.12	0.77
BNU-ESM	0.28	0.83	20	0.36	0.84
CanESM2	0.14	0.74	45	0.32	0.80
CCSM4	0.14	0.91	5	0.15	0.92
CESM1-BGC	0.14	0.90	0	0.14	0.90
CESM1-CAM5	0.16	0.85	0	0.16	0.85
CSIRO-Mk3-6-0	−0.06	0.28	0	−0.06	0.28
FGOALS-s2	0.18	0.89	60	0.45	0.93
GFDL-CM3	0.23	0.85	25	0.37	0.89
HadGEM2-ES	0.25	0.62	0	0.25	0.62
INMCM4	0.59	0.83	0	0.59	0.83
IPSL-CM5A-MR	0.02	0.04	95	0.14	0.12
MIROC-ESM-CHEM	0.23	0.85	0	0.23	0.85
MIROC-ESM	0.23	0.78	0	0.23	0.78
MPI-ESM-LR	0.16	0.70	40	0.31	0.73
MRI-CGCM3	0.08	0.04	0	0.08	0.04
NorESM1-M	0.12	0.79	0	0.12	0.79
NorESM1-ME	0.12	0.68	20	0.16	0.73

## Antarctic ice-discharge from SeaRISE response-functions

A. Levermann et al.

[Title Page](#)
[Abstract](#)
[Introduction](#)
[Conclusions](#)
[References](#)
[Tables](#)
[Figures](#)
[⏪](#)
[⏩](#)
[◀](#)
[▶](#)
[Back](#)
[Close](#)
[Full Screen / Esc](#)
[Printer-friendly Version](#)
[Interactive Discussion](#)

**Table 5.** East-Antarctic-Sea sector: scaling coefficients and time delay  $\Delta t$  between increase in global mean temperature and subsurface ocean temperature anomaly.

Model	Coeff. without $\Delta t$	$r^2$	$\Delta t$ [yr]	Coeff. with $\Delta t$	$r^2$
ACCESS1-0	0.20	0.92	30	0.35	0.94
ACCESS1-3	0.27	0.92	0	0.27	0.92
BNU-ESM	0.35	0.92	0	0.35	0.92
CanESM2	0.21	0.96	0	0.21	0.96
CCSM4	0.13	0.96	5	0.13	0.97
CESM1-BGC	0.12	0.94	25	0.17	0.95
CESM1-CAM5	0.15	0.94	0	0.15	0.94
CSIRO-Mk3-6-0	0.22	0.93	15	0.28	0.94
FGOALS-s2	0.17	0.90	55	0.41	0.94
GFDL-CM3	0.21	0.89	35	0.39	0.93
HadGEM2-ES	0.23	0.95	0	0.23	0.95
INMCM4	0.55	0.97	0	0.55	0.97
IPSL-CM5A-MR	0.14	0.89	0	0.14	0.89
MIROC-ESM-CHEM	0.11	0.89	0	0.11	0.89
MIROC-ESM	0.09	0.85	50	0.24	0.88
MPI-ESM-LR	0.20	0.94	15	0.26	0.95
MRI-CGCM3	0.26	0.94	0	0.26	0.94
NorESM1-M	0.15	0.76	0	0.15	0.76
NorESM1-ME	0.15	0.74	60	0.49	0.85

## Antarctic ice-discharge from SeaRISE response-functions

A. Levermann et al.

Title Page

Abstract

Introduction

Conclusions

References

Tables

Figures

⏪

⏩

◀

▶

Back

Close

Full Screen / Esc

Printer-friendly Version

Interactive Discussion

**Table 6.** Projections of ice-discharge in 2100 according to Fig. 11. Numbers are in meters sea-level equivalent for the different global climate RCP-scenarios with and without time delay  $\Delta t$ . The models PennState-3-D, PISM and SICOPOLIS have an explicit representation of ice-shelf dynamics and are denoted “shelf models”.

Set-up	RCP	Median	17 %	83 %	5 %	95 %
“Shelf models” with $\Delta t$	2.6	0.07	0.02	0.14	0.0	0.23
	4.5	0.07	0.03	0.16	0.01	0.27
	6.0	0.07	0.03	0.17	0.01	0.28
	8.5	0.09	0.04	0.21	0.01	0.37
“Shelf models” without $\Delta t$	2.6	0.09	0.04	0.17	0.02	0.25
	4.5	0.11	0.05	0.20	0.02	0.30
	6.0	0.11	0.05	0.21	0.02	0.31
	8.5	0.15	0.07	0.28	0.04	0.43
All models with $\Delta t$	2.6	0.08	0.03	0.17	0.01	0.27
	4.5	0.09	0.03	0.20	0.01	0.33
	6.0	0.09	0.03	0.20	0.01	0.34
	8.5	0.11	0.04	0.27	0.01	0.47
All models without $\Delta t$	2.6	0.11	0.05	0.19	0.02	0.29
	4.5	0.13	0.06	0.24	0.03	0.36
	6.0	0.13	0.06	0.25	0.03	0.38
	8.5	0.18	0.08	0.34	0.04	0.54

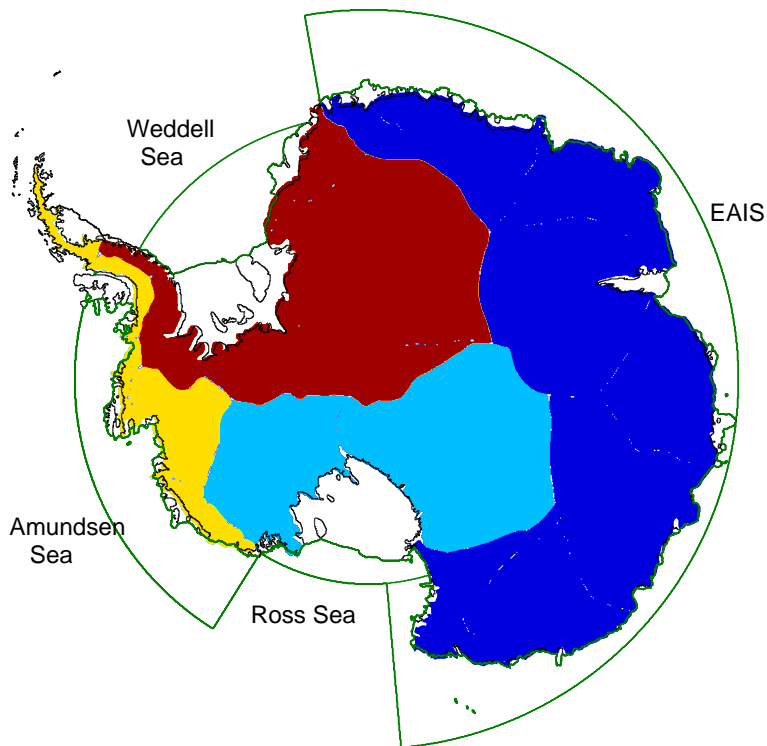


**Fig. 1.** The four different basins for which ice-sheet response functions are derived from the SeaRISE M2-experiments. Green lines enclose the oceanic regions over which the subsurface oceanic temperatures were averaged. Vertical averaging was carried out over a 100 m depth range centered at the mean depth of the ice-shelves in the region taken from Le Brocq et al. (2010) as provided in Table 1.

**Antarctic ice-discharge from SeaRISE response-functions**

A. Levermann et al.

Title Page

Abstract Introduction

Conclusions References

Tables Figures

⏪ ⏩

◀ ▶

Back Close

Full Screen / Esc

Printer-friendly Version

Interactive Discussion



## Antarctic ice-discharge from SeaRISE response-functions

A. Levermann et al.

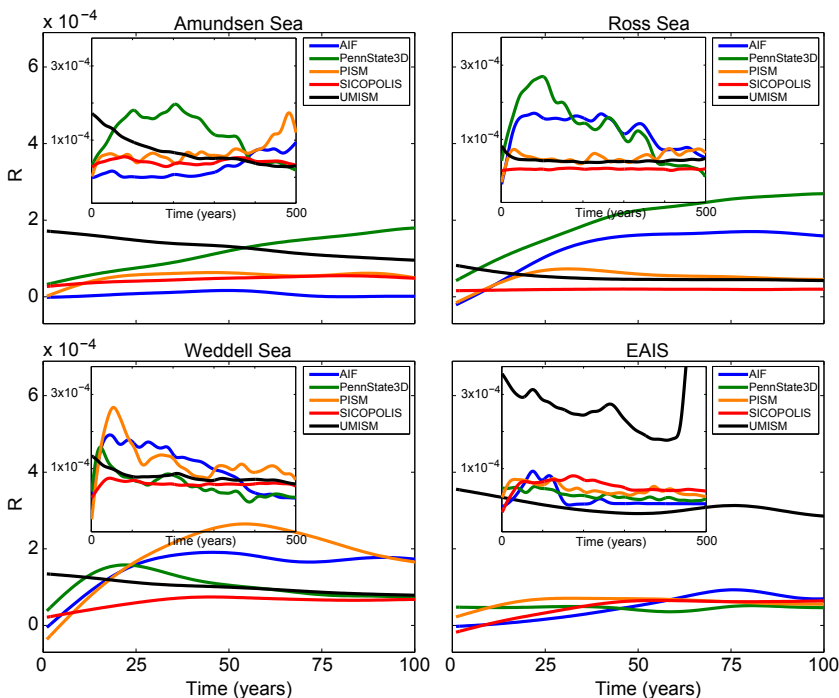


**Fig. 2.** Linear response functions for the five ice-sheet models of Antarctica for each region as defined by Eq. (4) and as obtained from the SeaRISE-M2-experiments. The projections up to the year 2100, as computed here, will be dominated by the response functions up to year 100 since this is the period of the dominant forcing. For completeness the inlay shows the response function for the full 500 yr, i.e. the period of the original SeaRISE experiments. As can be seen from Eq. (1), the response function is dimensionless. While the response functions are different for each individual basin and model when derived from the weaker M1-experiment (Fig. 13), the uncertainty range for the sea-level contribution in 2100 is very similar, since it is dominated by the uncertainty in climatic forcing (compare Fig. 10).

## Antarctic ice-discharge from SeaRISE response-functions

A. Levermann et al.

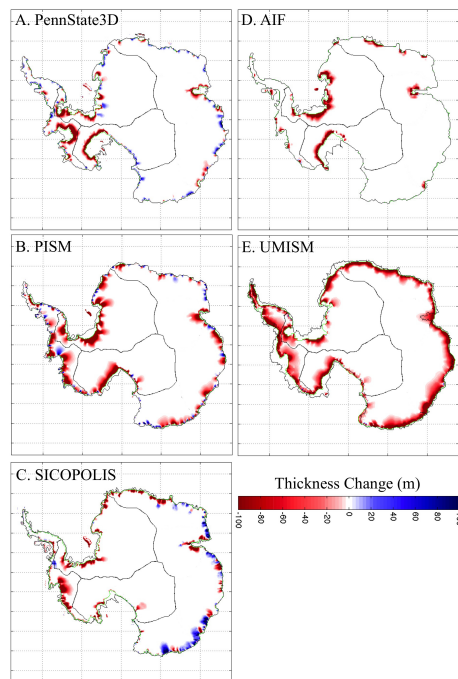


**Fig. 3.** Ice-thickness change after 100 yr under the SeaRISE experiment with homogeneous increase in basal ice-shelf melting of  $20 \text{ m a}^{-1}$  (experiment M2 and Fig. 13 in Nowicki et al., 2013a). Due to their coarse resolution some models with explicit representation of ice shelves such as the PISM model tend to underestimate the length of the coastline to which an ice shelf is attached which might lead to an underestimation of the ice loss. The UMISM model assumes basal melting along the entire coastline which is likely to result an overestimation of the effect. Black contours represent the initial grounding line which moved to the green contour during the M2-experiment after 100 yr. Lines within the continent show the drainage basins as in Fig. 1.

## Antarctic ice-discharge from SeaRISE response-functions

A. Levermann et al.

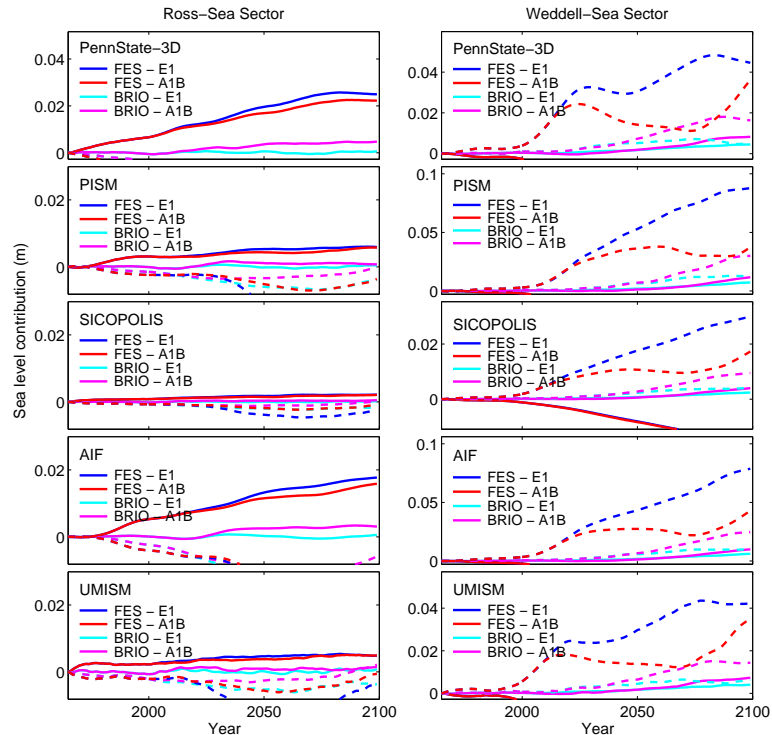


**Fig. 4.** Ice loss as obtained from forcing the five response functions (Fig. 2) with the basal melt rates from the high-resolution global finite-element model FESOM (FES) and the regional ocean model BRIOS (BRIO). The full lines represent simulations in which BRIOS and FESOM were forced with the global climate model ECHAM-5; dashed lines correspond to a forcing with the HadCM-3 global climate model. Results are shown for the strong climate-change scenario A1B and the relatively low-emission scenario E1. A medium basal melt sensitivity of  $11.5 \text{ ma}^{-1} \text{ K}^{-1}$  was applied. The results illustrate the important role of the global climatic forcing.

## Antarctic ice-discharge from SeaRISE response-functions

A. Levermann et al.

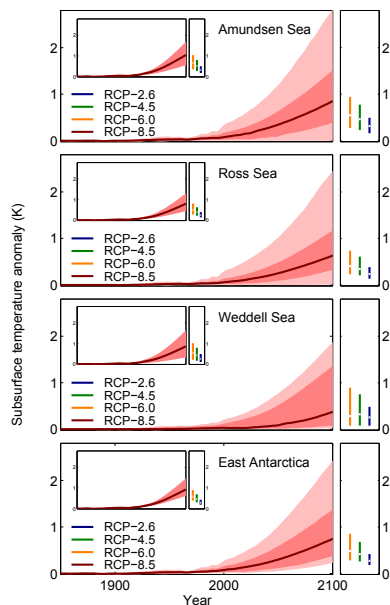


**Fig. 5.** Oceanic subsurface-temperature anomalies as obtained from scaling the range of global mean temperature changes under the different RCP scenarios to the oceanic subsurface outside the ice-shelf cavities. For the down-scaling the oceanic temperatures were diagnosed offshore of the ice-shelf cavities within the four regions defined in Fig. 1 at the depth of the mean ice-shelf thickness as defined in Table 1. These temperature anomalies were plotted against the global mean temperature increase for each of the 19 CMIP-5 climate models used here. The best scaling was obtained when using a time delay between global mean temperature and oceanic subsurface temperature anomalies. The scaling coefficients with the respective time delay are provided in Tables 2–5. The line corresponds to the median temperature evolution. The dark shading corresponds to the 66 % percentile around the median (red line). The light shading corresponds to the 99 % percentile. Inlays show the temperature anomalies without time delay.

## Antarctic ice-discharge from SeaRISE response-functions

A. Levermann et al.

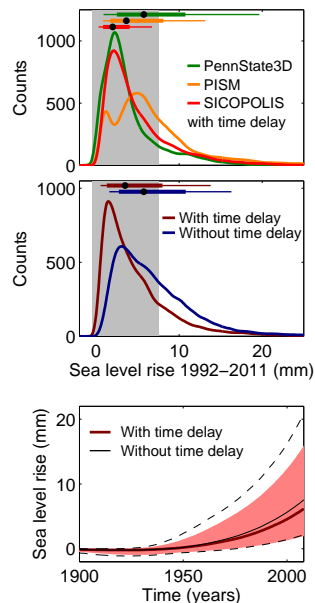


**Fig. 6.** Uncertainty range including climate, ocean and ice-sheet uncertainty for the projected change of the observational period 1992–2011. Upper panel: probability distribution for the three models with explicit representation of ice-shelves (PennState-3-D, PISM, SICOPOLIS). Middle panel: probability distribution with time delay (dark red) and without (dark blue) for three the models with explicit ice-shelf representation (“shelf models”). The gray shading in the upper two panels provide the estimated range from observations following Shepherd et al. (2012). The likely range obtained with time delay is almost identical with the observed range. All distributions are highly skewed towards high sea-level contributions which strongly influences the median (black dot at the top of the panel), the 66 %-range (thick horizontal line) and the 90 %-range (thin horizontal line). Lower Panel: time evolution for the hindcast projection using only the “shelf models”: with time delay, one obtains the red line as the median time series, the red shading provides the likely or 66 %-range. The black line shows the median without time delay together with the likely range for this case as dashed lines.

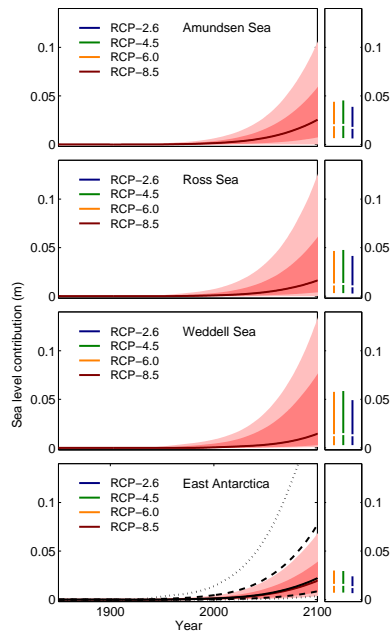


**Fig. 7.** Uncertainty range of contributions to global sea level from basal-melt induced ice discharge from Antarctica for the different basins. Results shown here include the three ice-sheet models with explicit representation of ice-shelf dynamics and the global climate forcing applied with a time delay as given in Table 2 – Table 5. The full red curve is the median enclosed by the dark shaded 66 %-range and the light shaded 99 %-range of the distribution for the RCP-8.5 scenario. Colored bars at the right show the other scenarios' 66 %-range intersected by the median. The full distribution is given in Fig. 8. The strongest difference between models with and without explicit representation of ice-shelves occurs in East Antarctica as exemplified in the lower panel. The dashed black line envelopes the 66 %-range of all models, the full black line is the median and the dotted line the 99 % percentile.

**Antarctic ice-discharge from SeaRISE response-functions**

A. Levermann et al.

Title Page

Abstract

Introduction

Conclusions

References

Tables

Figures

◀

▶

◀

▶

Back

Close

Full Screen / Esc

Printer-friendly Version

Interactive Discussion



## Antarctic ice-discharge from SeaRISE response-functions

A. Levermann et al.

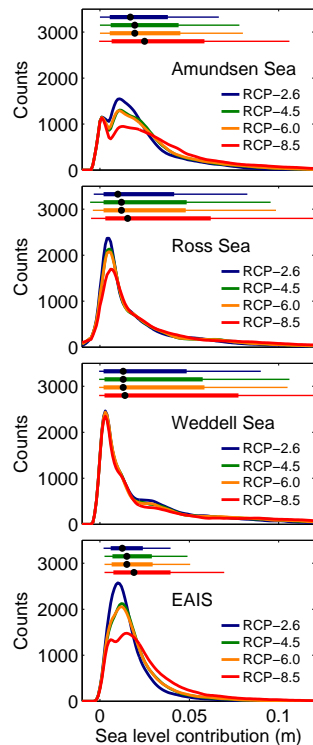


**Fig. 8.** Probability density function for the sea-level contribution from basal-melt-induced ice discharge for each region for the year 2100. Different colors represent the four RCP scenarios. Thick horizontal lines at the top of each panel provide the 66%-range of the distribution, the black dot is the median and the thin line the estimate of the 90%-range. Amundsen has the highest median contributions though sectors are relatively similar. Scenario dependency is strongest for the Amundsen region and East Antarctica. The distributions are highly skewed towards higher sea-level contributions. Results are shown for the models with explicit ice-shelf representation only.

[Title Page](#)
[Abstract](#)
[Introduction](#)
[Conclusions](#)
[References](#)
[Tables](#)
[Figures](#)
[⏪](#)
[⏩](#)
[◀](#)
[▶](#)
[Back](#)
[Close](#)
[Full Screen / Esc](#)
[Printer-friendly Version](#)
[Interactive Discussion](#)

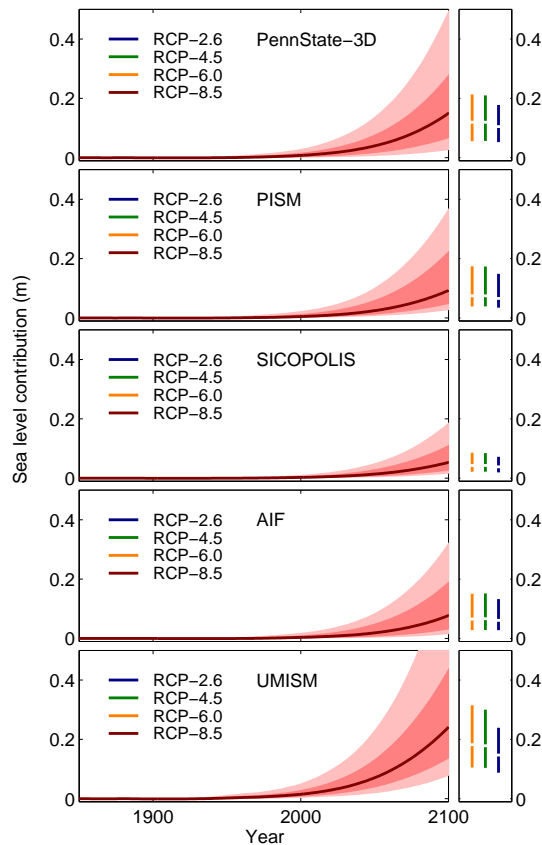


**Fig. 9.** Uncertainty range of contributions to global sea level from basal-melt induced ice discharge from Antarctica for the different ice-sheet models. Lines, shading and color coding as in Fig. 7. Colored bars at the right show the other scenarios' 66%-range intersected by the median.

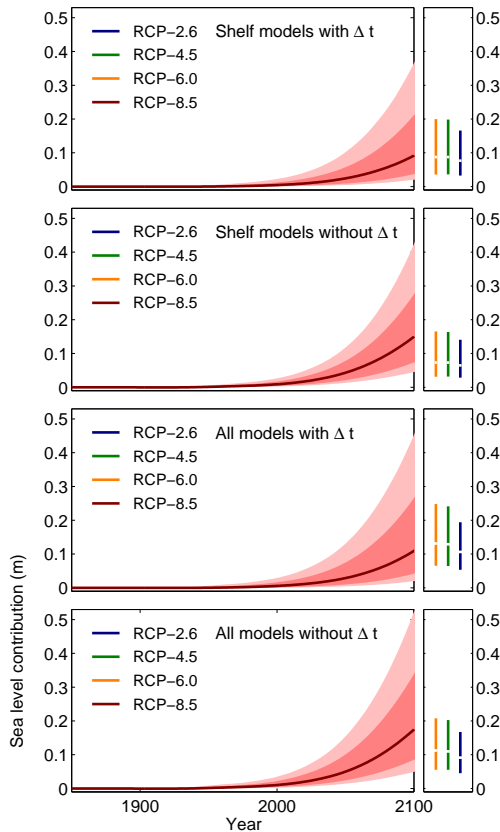


**Fig. 10.** Uncertainty range of contributions to global sea level from basal ice-shelf melt induced ice discharge from Antarctica including climate-, ocean- and ice-model uncertainty. Lines, shading and color coding as in Fig. 7. Estimates with and without the time delay between global mean surface air temperature and subsurface ocean temperature (Tables 2–5) are presented. “Shelf models” are those ice-sheet models with explicit representation of ice shelves.

**Antarctic ice-discharge from SeaRISE response-functions**

A. Levermann et al.

Title Page

Abstract Introduction

Conclusions References

Tables Figures

⏪ ⏩

⏴ ⏵

Back Close

Full Screen / Esc

Printer-friendly Version

Interactive Discussion



## Antarctic ice-discharge from SeaRISE response-functions

A. Levermann et al.

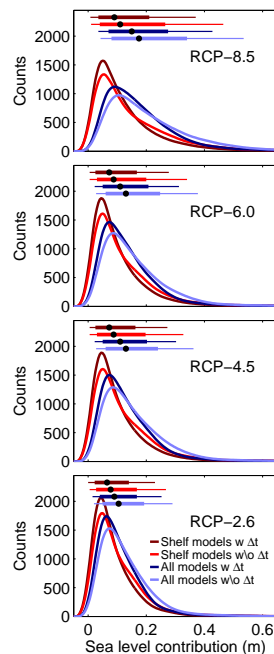


**Fig. 11.** Uncertainty range including climate, ocean and ice-sheet uncertainty. Different colors represent different setups for the total sea-level contribution from basal ice-shelf melt induced ice-discharge for the year 2100. Different panels provide estimates for the four RCP scenarios. Red curves in each panel show the three models with explicit representation of ice-shelves (PennState-3-D, PISM, SICOPOLIS). Blue curves show all models. Dark colors represent simulations using the time delay of Tables 2–5. Light colored lines give distributions without time lag. All distributions are highly skewed towards high sea-level contributions which strongly influences the median (black dot), the 66 %-range (thick horizontal line at top) and the 90 %-range (thin horizontal line at top). The scenario-dependence of each of these estimates is also visible in the number provided in Table 6.

[Title Page](#)
[Abstract](#)
[Introduction](#)
[Conclusions](#)
[References](#)
[Tables](#)
[Figures](#)
[⏪](#)
[⏩](#)
[◀](#)
[▶](#)
[Back](#)
[Close](#)
[Full Screen / Esc](#)
[Printer-friendly Version](#)
[Interactive Discussion](#)

## Antarctic ice-discharge from SeaRISE response-functions

A. Levermann et al.

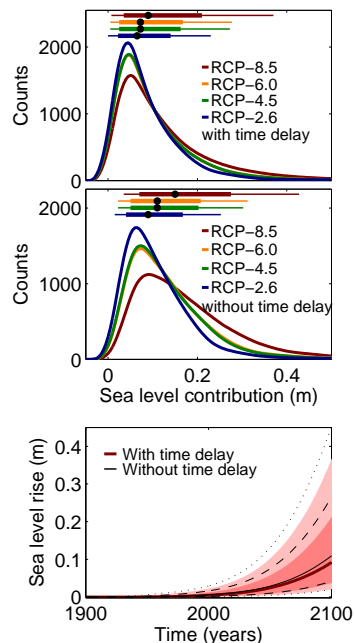


**Fig. 12.** Uncertainty range including climate, ocean and ice-sheet uncertainty for the year 2100. Different colors represent different scenarios using the three models including an explicit representation of ice shelves (PennState-3-D, PISM, SICOPOLIS). The upper panel shows the results with time delays as listed in Tables 2–5. The middle panel shows the results without this time delay. All distributions are highly skewed towards high sea-level contributions which strongly influences the median, the 66%-range (thick horizontal line at the top of the panel) and the 90%-range (thin horizontal line at the top of the panel). The scenario-dependence is strongest in the higher percentile of the distribution as also visible in the numbers provided in Table 6. The lower panel shows the corresponding time series of the median, the 66%- and the 90%-percentile of the distribution with and without time delay.

## Antarctic ice-discharge from SeaRISE response-functions

A. Levermann et al.

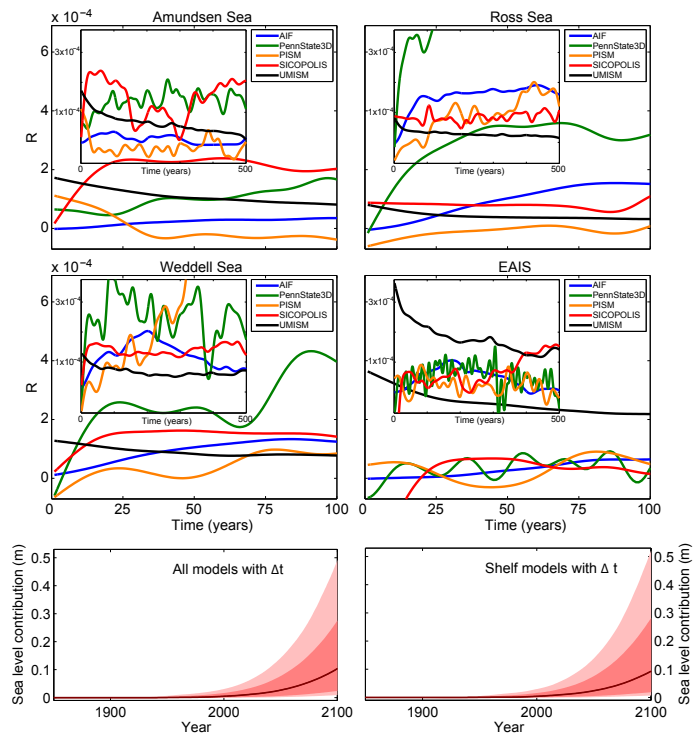


**Fig. 13.** Response functions as obtained from the M1-experiment of the SeaRISE intercomparison with an additional uniform basal ice-shelf melting of  $2 \text{ ma}^{-1}$ . The upper four panels correspond to Fig. 2. The lower two panels show the uncertainty range in sea-level projections with the M1-response-functions from above. The ranges obtained are very similar to the ranges obtained with the M2-response-functions as shown in Fig. 10. While the response functions are very different for the M1 experiment compared to the M2 experiment, the projected ranges of sea level rise are similar which is consistent with the fact that the uncertainty arises mainly from the uncertainty in the external forcing of the ice-sheets.